


# Development of an in situ polymerized artificial layer for dendrite-free and stable lithium metal batteries

Junquan Lai<sup>1,2</sup> | Rui Tan<sup>3</sup>  | Huai Jiang<sup>1,2</sup> | Xinjing Huang<sup>1,2</sup> |  
Zhongliang Tian<sup>1,2</sup> | Bo Hong<sup>1,2</sup> | Mengran Wang<sup>1,2</sup> | Jie Li<sup>1,2</sup>

<sup>1</sup>School of Metallurgy and Environment, Central South University, Changsha, Hunan, China

<sup>2</sup>National Engineering Research Center of Advanced Energy Storage Materials, Changsha, Hunan, China

<sup>3</sup>Warwick Electrochemical Engineering, WMG, University of Warwick, Coventry, UK

## Correspondence

Rui Tan, Warwick Electrochemical Engineering, WMG, University of Warwick, Coventry, CV4 7AL, UK.  
Email: [rui.tan@warwick.ac.uk](mailto:rui.tan@warwick.ac.uk)

Bo Hong and Mengran Wang, School of Metallurgy and Environment, Central South University, Changsha 410083, Hunan, China.

Email: [bop\\_hong@csu.edu.cn](mailto:bop_hong@csu.edu.cn) and [mengranwang93@163.com](mailto:mengranwang93@163.com)

## Funding information

Warwick Manufacturing Group at the University of Warwick; National Natural Science Foundation of China, Grant/Award Number: 52034011; RSC Researcher Collaborations Grant, Grant/Award Number: C23-8220221815

## Abstract

Severe lithium dendrite issues bring a significant challenge for the practical application of Li metal anodes. In this study, a scalable spray-coating method is used to in situ construct an organic/inorganic composite interfacial layer including Li-Zn alloy and lithium polyacrylate on the surface of lithium metal. The Li-Zn alloy exhibits favorable lithiophilic and high Li<sup>+</sup> diffusion coefficient, whereas highly elastic lithium polyacrylate is a Li<sup>+</sup> conductor and provides excellent mechanical properties. Finally, the ZA-Li||ZA-Li cell shows stable cycling for over 1800 h with 1 mA cm<sup>-2</sup> at 2 h per cycle, which demonstrates a pronounced inhibition of lithium dendrite growth. Based on the above merits, this work would open a new avenue to develop advanced artificial interfacial layer with multiple capabilities for high-performance lithium metal batteries.

## KEYWORDS

alloy, interfacial layer, lithium metal anode, metallic dendrite, organic/inorganic solid interface

## 1 | INTRODUCTION

Lithium metal batteries (LMBs) with a high energy density have become a variable solution towards global carbon neutrality and net-zero emissions. However, two major challenges are involved in the commercialization of LMBs, that is, lithium dendrite and low Coulombic efficiency attributing to the nature of highly redox-reactive Li metal.<sup>1–3</sup>

Li metal with high reactivity potentially induces the side reactions of organic electrolyte and produce decomposition products, for example, Li<sub>2</sub>O, Li<sub>2</sub>CO<sub>3</sub>, LiF, LiOH, and

RCOOLi, leading to the formation of nonuniform solid electrolyte interface (SEI) on the Li metal. In this scenario, uneven stripping and plating of Li<sup>+</sup> tends to occur on the surface of Li metal<sup>4</sup> and results in the growth of needle-like or mossy-like metallic dendrites (Figure 1A).<sup>5,6</sup> The formed SEI layers lack sufficient mechanical robustness to alleviate the penetration of Li dendrites.<sup>7</sup> Given these challenges, developing a uniform and mechanically robust interface layer is highly required for stable and safe LMBs.

Considerable research efforts have been made to enhance the properties of constructed interfacial layers, such as establishing ex situ artificial solid interface,

This is an open access article under the terms of the [Creative Commons Attribution](https://creativecommons.org/licenses/by/4.0/) License, which permits use, distribution and reproduction in any medium, provided the original work is properly cited.

© 2024 The Authors. *Battery Energy* published by Xijing University and John Wiley & Sons Australia, Ltd.

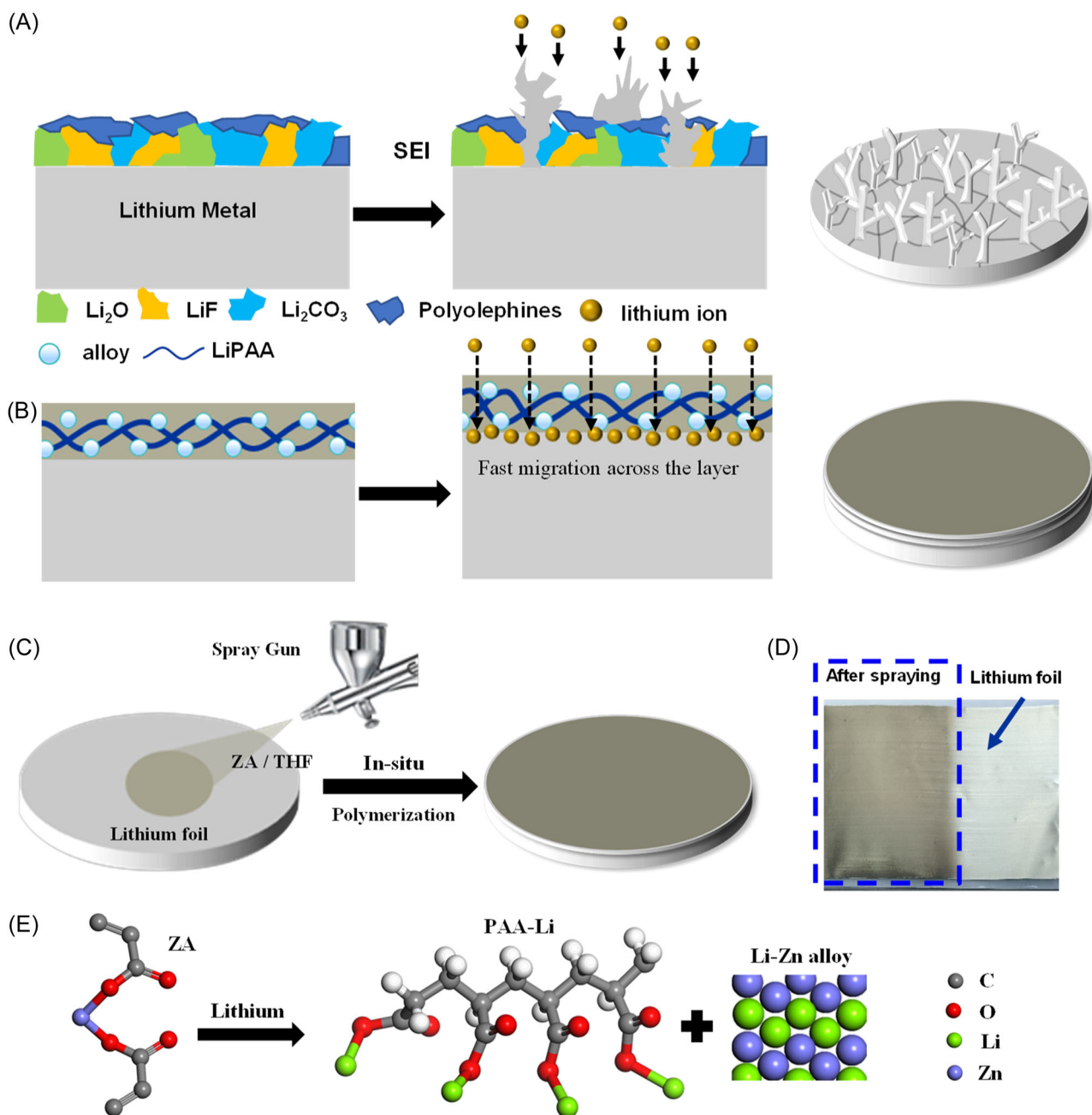


**FIGURE 1** (A) Scheme showing the principles of dendrite growth on the surface of Li metal. (B) Working mechanism of an in situ established alloy-polymer protective layer. (C) Schematic diagram of the preparation process of alloy-polymer layers. (D) Optical images of Li foil before and after zinc acrylate (ZA) spraying. (E) Reaction mechanism of the alloy-polymer layer. LiPAA, lithium polyacrylate; SEI, solid electrolyte interface.

developing new chemistries of electrolytes and additives, as well as tuning the composition of electrolytes.<sup>8,9</sup> Preparation of interfacial layer on lithium anode is a straightforward and facile protocol to improve the stability of SEI and suppress the growth of Li dendrite. In terms of the material chemistries, coating materials generally include inorganics, for example, lithium nitride,<sup>10,11</sup> lithium fluoride,<sup>12–15</sup> lithium silicate,<sup>16</sup> and lithium phosphate,<sup>17</sup> and organics, for example, silane-based

materials,<sup>18,19</sup> polyvinylidene fluoride,<sup>20–22</sup> cyclic ethers polymer,<sup>23</sup> and lithium polyacrylate.<sup>24,25</sup> Fabricating coating layers by using inorganic and organic composite materials have emerged as a new strategy which combines the fast  $\text{Li}^+$ -ion transport ability of inorganic materials and the flexibility of organic polymers,<sup>26–29</sup> such as lithiophilic–lithophobic interface layers.<sup>30</sup> Although the new strategies demonstrate significant progress, the complicated process of making inorganic and organic

interfacial layers challenge its practical deployment. Developing a simple protocol for interfacial engineering is substantially important.

In this work, we propose a facile strategy of fabricating organic-inorganic composite interface layer for alleviating the growth of Li dendrite and enabling improved battery cycling. We demonstrate this approach by simply reducing zinc acrylate (ZA) with reactive Li metal at room temperature to afford Li<sup>+</sup>-ion-conductive LiZn alloy particles, which are embedded in a self-polymerized lithium polyacrylate (LiPAA) matrix (Figure 1B).<sup>27,31–33</sup> This artificial interface layer features abundant Li<sup>+</sup>-ion migration channels and remarkable flexibility, which can effectively suppress the growth of lithium dendrites and deliver a long-cycling performance of 1800 h for Li||Li symmetric cells at 1.0 mA cm<sup>-2</sup> with a small lithium electroplating/stripping overpotential of around 50 mV. Paired with lithium iron phosphate, interfacial-engineered anodes enabled full cells to achieve improved cycling performance over 450 cycles at 1.0 C.

## 2 | RESULTS AND DISCUSSIONS

To demonstrate our strategy, a tetrahydrofuran solution of zinc acrylate was simply sprayed onto the surface of the lithium foil at room temperature (Figure 1C). The spontaneous reaction underwent between the zinc acrylate solution and reactive Li metal, which was evidenced by the color alteration of Li metal surface (Figure 1D,E). X-ray diffraction was performed to characterize the phase composition of the formed interfacial film (Figure 2A). Compared with pristine lithium, four typical characteristic peaks were observed at 24.7° and 40.9°, referring to the LiZn alloy (LiZn, PDF#03-0954), and 38.99° and 43.23°, corresponding to zinc metal (Zn, PDF#04-0831). Several unmatched peaks are impurities generated during sample preparation and transfer, such as Li<sub>2</sub>CO<sub>3</sub> (21.22°). Chemical composition of this interfacial film was investigated by Fourier transformation infrared spectroscopy (Figure 2B), in which the characteristic peaks of C=C at 1643 cm<sup>-1</sup> are greatly reduced, indicating the C=C bonds underwent a self-polymerization reaction induced and catalyzed by the reactive Li metal.<sup>34</sup> The reaction between zinc acrylate and Li metal was clearly proved by X-ray photoelectron spectroscopy (XPS). It can be clearly observed that the alloy phase LiZn is formed on the surface of the lithium sheet (Figure 2C), while the characteristic peak of -COO- is derived from Li-PAA (Figure 2D), which also provides some potential transport channels for Li<sup>+</sup> within the polymer matrix. The deeper XPS pattern (100 s sputtering) further verified the enrichment of -COOLi groups and the uniform distribution of the LiZn alloy (Supporting Information S1: Figure S1).

The morphology and chemical composition of the artificial interface layer was characterized by scanning electron microscopy (SEM). As shown in Figure 2F, a dense and uniform coating layer was detected without any observable defects and cracks. After comparison with pristine Li (Supporting Information S1: Figure S2), it can be determined that the thickness of this interfacial layer is about 1.0 μm (Figure 2G), which barely increases the weight of Li metal and sacrifices the gravimetric energy density. The energy spectrum shows the uniform distribution of C and Zn in this layer (Figure 2G). This uniform layer will benefit the even transport of ions and alleviate the growth of dendrites. In contrast, a mossy-like surface was observed for pristine Li metal (Figure 2E and Supporting Information S1: Figure S3), of which this type of morphology inclines to induce the uneven stripping and plating of Li<sup>+</sup> and produce Li dendrite. We therefore successfully fabricate an organic (Li-PAA)-inorganic (LiZn) composite interfacial layer by using a simple spraying coating technique. The uniform and defect-free interfacial layer is anticipated to play an important role in inhibiting the growth of Li dendrites and stabilizing the battery cycling.

To prove the function of interface-engineered Li anodes in preventing the growth of Li dendrites, we built up symmetrical Li||Li cell to evaluate the cycle durability. Figure 3A and Supporting Information S1: Figure S4 shows the cycling profiles of ZA-Li and bare Li anodes with an area capacity of 1.0 mAh cm<sup>-2</sup> at current densities of 1.0 and 3.0 mA cm<sup>-2</sup>, respectively. At 1.0 mA cm<sup>-2</sup>, the lithium electroplating/stripping overpotential of a cell (>120 mV) with bare Li metals increases substantially after 400 h. In comparison, the symmetrical cell with ZA-Li anodes delivered a stable cycling performance of over 1800 h with a small lithium electroplating/stripping overpotential of around 50 mV. At 3.0 mA cm<sup>-2</sup> (Supporting Information S1: Figure S2), the interface-engineered Li anodes clearly exhibited excellent cycle stability of over 1200 h, much superior to that of the bare Li anodes (200 h). These results clearly confirm that the organic-inorganic interfacial layer can enable a uniform and fast ion transport, and elongate the life of Li anodes. Of particular interest is the lithium polyacrylate component that can effectively enhance the flexibility and mechanical robustness of this layer, thus alleviating the issue of the transformation and fracture of this interface layer over cycling. The electrochemical impedance spectrum (EIS) of Li/Li symmetrical cells after varied cycles are conducted (Supporting Information S1: Figure S5). The interface resistance of pristine Li is always larger (~140 Ω) and increases gradually after cycling because of the accumulation of SEI layers. In comparison, the ZA-Li symmetrical cells have a larger electrochemical impedance at the beginning of cycling and it gradually

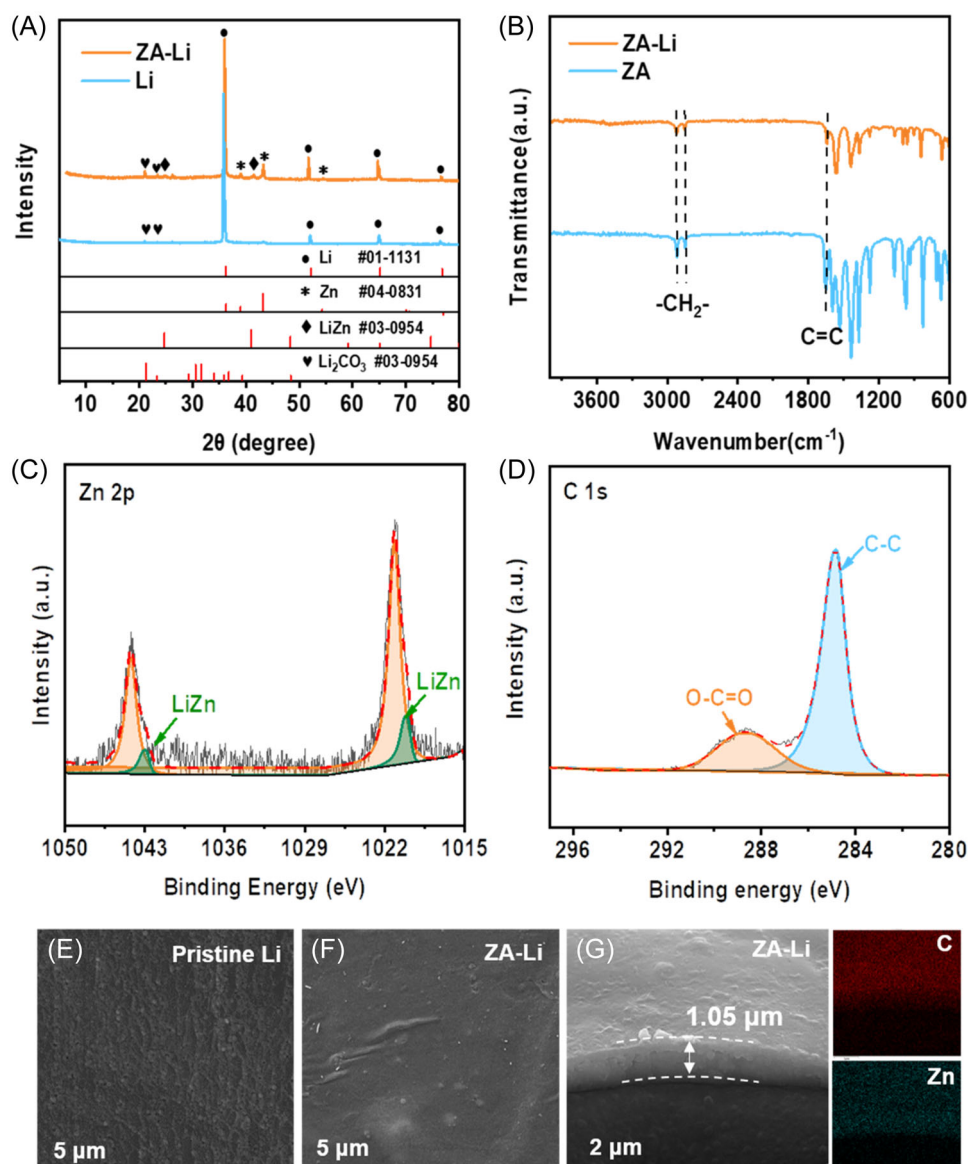


**FIGURE 2** (A) X-ray diffraction patterns of the pristine Li and ZA-Li. (B) Fourier transformation infrared spectrum of the treated Li and ZA-Li. X-ray photoelectron spectroscopy spectra of zinc acrylate (ZA)-coated anode, including (C) Zn 2p; (D) C 1s. Scanning electron microscopy (SEM) images of Li anodes and ZA-coated Li: top view of (E) pristine Li and (F) ZA-Li. Cross-sectional SEM images of (G) ZA-Li anode and energy spectrum of C element; Zn element.

decreases to a stable value, which may be attributed to the activation and stabilization of the ZA layer. After 50 cycles, the treated Li manifested lower interfacial charge transfer resistance as compared with the pristine Li owing to the fast  $\text{Li}^+$  transport channels provided by the LiZn alloy. To further quantify the lithium-ion conductivity of the composite interface layer, additional processing of EIS data from uncycled ZA-Li symmetric cells was conducted. Subsequently, an equivalent circuit and physical model of the SEI were developed, as depicted in Supporting Information S1: Figure S6A, based on relevant literature.<sup>35</sup> Fitting was performed in the high-frequency range, excluding the outer layer portion associated with the liquid

electrolyte. The results in Figure S6B exhibit excellent consistency between the fitting results using the aforementioned model and the EIS data. The obtained value of  $R_{\text{SEI}}$  is  $78.65 \Omega$ , resulting in a calculated lithium-ion conductivity of the composite interface layer of  $1.651 \times 10^{-5} \text{ S cm}^{-1}$ .

Furthermore, the activation energies ( $E_a$ ) were estimated by fitting the EIS of Li | Li symmetric cells at varied temperatures (Supporting Information S1: Figure S7). For the interface-engineered Li anodes, the  $E_a$  value is as small as  $52.98 \text{ kJ mol}^{-1}$  with a good linear fitting effect according to the Arrhenius equation (Figure 3C). In comparison, the bare Li anodes exhibit an  $E_a$  value of  $69.55 \text{ kJ mol}^{-1}$ , indicating that the interfacial layer

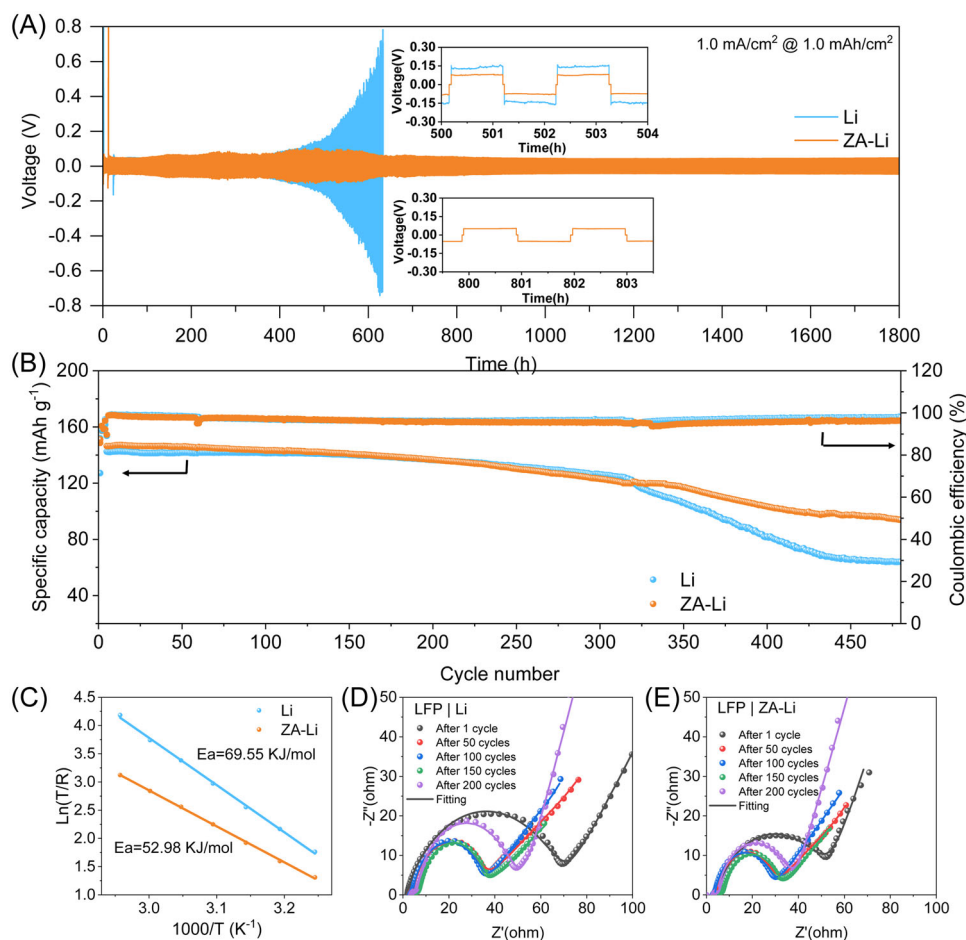


**FIGURE 3** (A) Stability of electrochemical plating-stripping process of Li metal anodes in symmetric cells at current densities of 1.0 mA cm<sup>-2</sup>. (B) Cycling performance of LiFePO<sub>4</sub>||Li full cells using pristine Li and ZA-Li anodes. (C) Arrhenius plot and their linear fitting to disclose the activation energy; electrochemical impedance spectrum (EIS) plots of LiFePO<sub>4</sub>||Li cells using (D) pristine Li and (E) ZA-Li anodes after different cycles. LFP, LiFePO<sub>4</sub>.

facilitates improved interfacial dynamics, enhanced charge transfer ability and stable electrode cycling. The chemical compositions on the surface of the Li and ZA-Li are further analyzed by the XPS spectrum after 50 cycles. As shown in Supporting Information S1: Figure S8A, the carbon-based peaks including COR, COOR, and C-F. The C-F peak increase markedly on the surface of pristine Li after cycles because of the side reactions between Li metal and electrolyte. In contrast, no obviously change on the surface composition of Li-PAA-Li anode and was still dominated by COOR (Supporting Information S1: Figure S8B). It is proved that the composite interface layer can stabilize Li anode and suppress side reactions between fresh Li and electrolyte markedly.

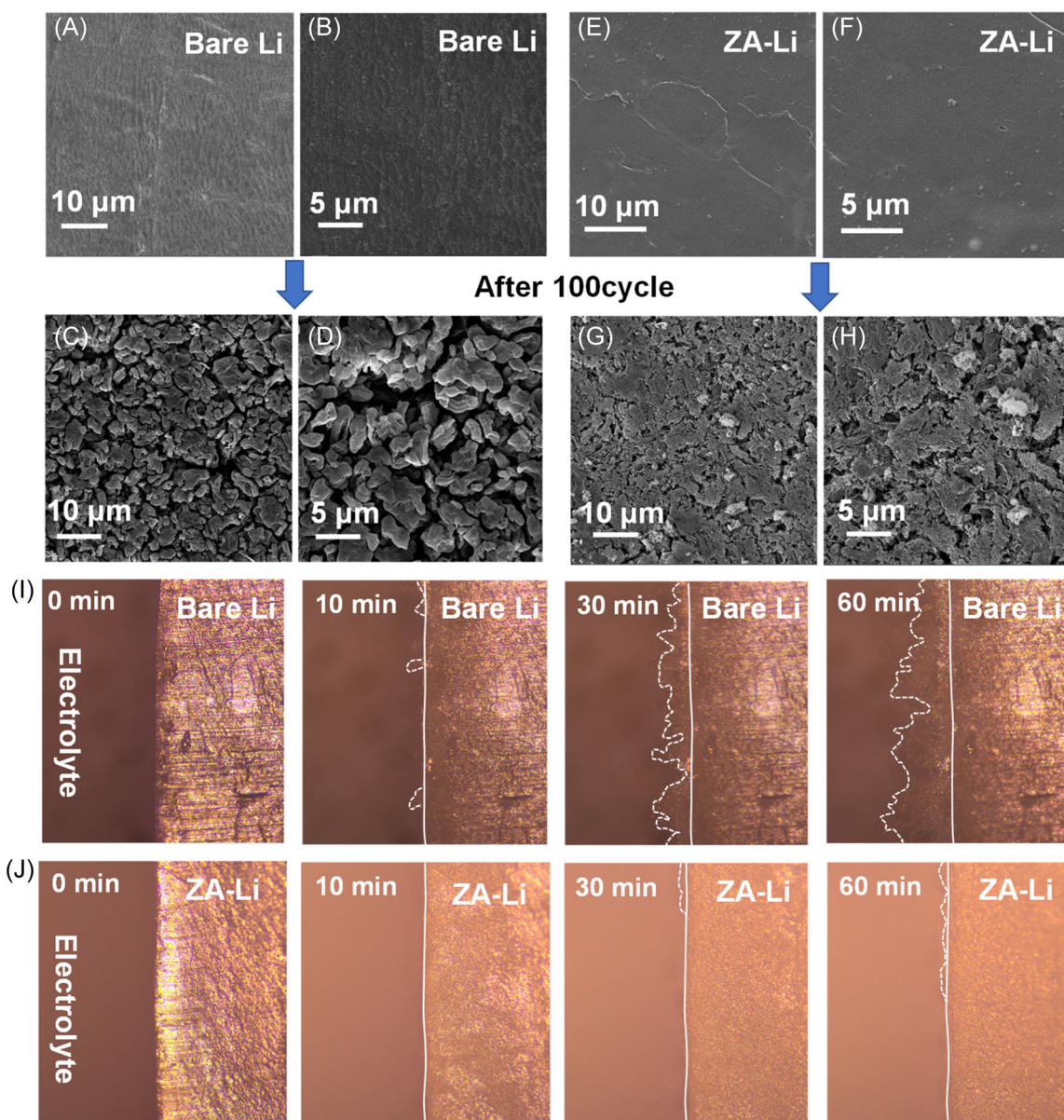
Lithium iron phosphate is currently widely used as a cathode material for lithium batteries. Here, we employ the modified ZA-Li anode to match the LiFePO<sub>4</sub> (LFP) cathode to further investigate the performance of ZA-Li anode in the full cells at the rate of 1C (1C = 170 mAh g<sup>-1</sup>).

Figure 3B and Supporting Information S1: Figures S9 and S10 show that the LFP/ZA-Li battery has 146 mAh g<sup>-1</sup> discharge capacity at the first cycle and 98 mAh g<sup>-1</sup> after 450 cycles with capacity retention of 67.1%. However, after the same cycle, the discharge capacity of the LFP/Li battery is only 63.6 mAh g<sup>-1</sup> and the retention rate is about 43.6%. The rate performance of the full cells was tested over a range of 0.2C to 5C (Supporting Information S1: Figure S11). Both cells exhibited similar discharge capacities at 0.2C (LFP||ZA-Li: 151.4 mAh g<sup>-1</sup>; LFP||Li: 148.2 mAh g<sup>-1</sup>). However, the capacity of LFP||Li cells decreases rapidly and the disparity with LFP||ZA-Li cells widens as the current density increases. The LFP||Li cell only achieves a discharge capacity of 77.4 mAh g<sup>-1</sup> at 5C, whereas its counterpart can still deliver 96.3 mAh g<sup>-1</sup>. The EIS of full cells after varied cycles are conducted (Figure 3D,E). The semicircle obtained in the high frequency range can be ascribed to the SEI and charge-transfer resistance. After one cycle, the LFP||ZA-Li cells

show a less resistance ( $48.6 \Omega$ ) compared to pristine LFP||Li ( $68.1 \Omega$ ). Throughout the cycle, LFP||ZA-Li consistently demonstrates a lower level of resistance. Furthermore, there is a more significant increase in the resistance of LFP||Li after 200 cycles. These results indicate that the ZA-Li anode has excellent stability in a commercial carbonate electrolyte. We conducted a CV experiment of Li|Cu and ZA-Li|Cu half cells within the  $-0.1$  to  $0.4$  V voltage range (Supporting Information S1: Figure S12). The results show that after the interface layer is modified, the current response of the ZA-Li surface only decreases slightly, which is consistent with quick  $\text{Li}^+$  transport. Furthermore, the cycle reversibility of the modified lithium anode has

been greatly improved, verifying the stability of the interface layer.

To visualize the function of the inhibited growth of Li dendrites by our developed organic-inorganic interfacial layers, we performed SEM and optical microscope to the electrodeposition of  $\text{Li}^+$  (Figure 4). After 100 cycles at  $1.0 \text{ mA cm}^{-2}$  ( $1.0 \text{ mAh cm}^{-2}$ ), numbers of loose and porous dendrites were formed on the surface of Li metal (Figure 4C,D). Cavities among these dendrites undesirably provide more space for the side reactions between liquid organic electrolytes and Li metal, accelerating the production of dead lithium and causing the failure of the



**FIGURE 4** Scanning electron microscopy (SEM) images of Li anodes before and after 100 cycles. Top view SEM images of Bare Li anode: (A, B) Before cycle and (C, D) after cycle. Top view SEM images of ZA-Li anode: (E, F) Before cycle; (G, H) after cycle. Photographs taken at different intervals of (I) Bare Li and (J) treated Li at  $2.0 \text{ mA cm}^{-2}$ . The scale bars are  $100 \mu\text{m}$  in (I and J).

Li anode. In contrast, after 100 cycles, the interface-engineered Li anodes maintain a relatively flat surface with much less cracks and voids (Figure 4G,H). In-situ observation of the growth of Li dendrites was carried out with an optical microscope (Figure 4I,J). Both anodes were encapsulated within transparent and sealed cells to rule out the effects of air. In contrast to the smooth and flat surface, needle-like dendrites formed on the bare Li anode after 10 min at  $2.0 \text{ mA cm}^{-2}$  (Figure 4I). Subsequently,  $\text{Li}^+$  preferentially deposited on these needles, leading to the formation of large and sharp protrusions. Compared with bare Li anodes, our developed interfacial layer maintained a smooth surface of Li metals without any observable dendrites (Figure 4J). These results strongly prove the effective function of this interfacial layer on the prevention of Li dendrites.

The working principles as proposed in Figure 1A,B are clearly evidenced by the aforementioned experimental results. In native SEI, which was generated by the reaction of lithium metal with electrolytes, due to the nonuniform distribution of inorganic–organic components, there is local aggregation during the migration of  $\text{Li}^+$ , which inevitably induces the growth of lithium dendrites. Since the native SEI does not have sufficient mechanical strength, sharp Li dendrites can easily pierce the native SEI, resulting in dead lithium lacking electrical contact, and even piercing the separator to short-circuit the battery. This process will continue to consume the electrolyte and active metal lithium, eventually leading to battery failure (Figure 3A,B). For the metal lithium anode modified by the composite interface layer, in the preformed interface layer, the ester group on the polymer backbone has a strong polarity and can attract  $\text{Li}^+$ .<sup>36</sup> When the electrolyte infiltrates the interface layer, the ester group can induce uniform redistribution of lithium ions within it. In addition, the insulating lithium polyacrylate enables the composite layer to have sufficient electron transfer resistance, as shown by some amorphous carbon and graphene,<sup>37</sup> to avoid the discharge deposition of  $\text{Li}^+$  above the film. Furthermore, an electric field is established across the film, which powers the passage of lithium ions through the protective layer. The LiZn alloy composition, which is uniformly coated with organic matter and dispersedly distributed, has a high lithium ion diffusion coefficient ( $4.7 \times 10^{-8} \text{ cm}^2 \text{ s}^{-1}$ ),<sup>31</sup> which is conducive to the rapid transport of  $\text{Li}^+$  in the interface layer.  $\text{Li}^+$  will be deposited under the film layer under the combined action of the components of the interface film, and finally the smooth deposition of lithium metal is realized.

### 3 | CONCLUSIONS

In this work, we constructed an organic/inorganic solid interface layer on the surface of the lithium metal anode through a simple spraying method to achieve the dendrite-free morphology of the metal lithium anode. The LiZn alloy component in the interface layer acts as an ion conductive channel to guide the uniform migration of  $\text{Li}^+$ , thereby inhibiting the growth of lithium dendrites. The in-situ formed polyacrylic acid lithium polymer effectively improves the flexibility of the interface layer, slowing down the interface layer damage problem. Moreover, the ester groups on the polymer backbone have strong polarity, which can attract  $\text{Li}^+$  and induce uniform redistribution of lithium ions. Taking advantage of the ZA composite interface layer, the lithium anode protected by the coating has excellent electrochemical performance. The symmetrical battery with ZA-protected lithium negative electrode exhibits enhanced stability of the stripping/plating process at a current density of  $1.0 \text{ mA cm}^{-2}$ , with its cycle time exceeding 1800 h. This simple yet effective approach may promote the commercialization of Li metal batteries.

### ACKNOWLEDGMENTS

The authors acknowledge the support from Warwick Manufacturing Group at the University of Warwick, the National Natural Science Foundation of China (52034011), and the RSC Researcher Collaborations Grant (C23-8220221815).

### CONFLICT OF INTEREST STATEMENT

The authors declare no conflict of interest.

### DATA AVAILABILITY STATEMENT

Data available on request from the authors.

### ORCID

Rui Tan  <http://orcid.org/0009-0001-9278-7327>

### REFERENCES

1. Wood KN, Noked M, Dasgupta NP. Lithium metal anodes: toward an improved understanding of coupled morphological, electrochemical, and mechanical behavior. *ACS Energy Lett.* 2017;2:664-672.
2. Zhang SS. Problem, status, and possible solutions for lithium metal anode of rechargeable batteries. *ACS Appl Energy Mater.* 2018;1:910-920.
3. Kornilov D, Penki TR, Cheglakov A, Aurbach D. Li/graphene oxide primary battery system and mechanism. *Battery Energy.* 2022;1:20210002.
4. Kim S-H, Choe U-J, Kim N-Y, Lee S-Y. Fibrous skeleton-framed, flexible high-energy-density quasi-solid-state lithium metal batteries. *Battery Energy.* 2022;1:20210012.

5. Gao P, Zhang C, Wen G. Equivalent circuit model analysis on electrochemical impedance spectroscopy of lithium metal batteries. *J Power Sources*. 2015;294:67-74.
6. Tasaki K, Goldberg A, Lian JJ, Walker M, Timmons A, Harris SJ. Solubility of lithium salts formed on the lithium-ion battery negative electrode surface in organic solvents. *J Electrochem Soc*. 2009;156:A1019-A1027.
7. Bieker G, Winter M, Bieker P. Electrochemical in situ investigations of SEI and dendrite formation on the lithium metal anode. *Phys Chem Chem Phys*. 2015;17:8670-8679.
8. Lin D, Liu Y, Cui Y. Reviving the lithium metal anode for high-energy batteries. *Nat Nanotechnol*. 2017;12:194-206.
9. Cheng XB, Zhang R, Zhao CZ, Zhang Q. Toward safe lithium metal anode in rechargeable batteries: a review. *Chem Rev*. 2017;117:10403-10473.
10. Li Y, Sun Y, Pei A, et al. Robust pinhole-free  $\text{Li}_3\text{N}$  solid electrolyte grown from molten lithium. *ACS Cent Sci*. 2018;4:97-104.
11. Zhang YJ, Wang W, Tang H, et al. An ex-situ nitridation route to synthesize  $\text{Li}_3\text{N}$ -modified Li anodes for lithium secondary batteries. *J Power Sources*. 2015;277:304-311.
12. Yuan Y, Wu F, Chen G, Bai Y, Wu C. Porous LiF layer fabricated by a facile chemical method toward dendrite-free lithium metal anode. *J Energy Chem*. 2019;37:197-203.
13. Zhang XQ, Chen X, Cheng XB, et al. Highly stable lithium metal batteries enabled by regulating the solvation of lithium ions in nonaqueous electrolytes. *Angew Chem Int Ed*. 2018;57:5301-5305.
14. Chen J, Fan X, Li Q, et al. Electrolyte design for LiF-rich solid-electrolyte interfaces to enable high-performance micro-sized alloy anodes for batteries. *Nat Energy*. 2020;5:386-397.
15. Qiu Z, Shen S, Liu P, et al. Plasma enhanced lithium coupled with cobalt fibers arrays for advanced energy storage. *Adv Funct Mater*. 2023;33:2214987.
16. Long K, Huang S, Wang H, et al. Green mechanochemical Li foil surface reconstruction toward long-life Li-metal pouch cells. *Energy Environ Sci*. 2024;17:260-273.
17. Bai M, Xie K, Hong B, et al. An artificial  $\text{Li}_3\text{PO}_4$  solid electrolyte interphase layer to achieve petal-shaped deposition of lithium. *Solid State Ionics*. 2019;333:101-104.
18. Wu M, Wen Z, Jin J, Chowdari BVR. Trimethylsilyl chloride-modified Li anode for enhanced performance of Li-S cells. *ACS Appl Mater Interfaces*. 2016;8:16386-16395.
19. Zhu B, Jin Y, Hu X, et al. Poly(dimethylsiloxane) thin film as a stable interfacial layer for high-performance lithium-metal battery anodes. *Adv Mater*. 2017;29:1603755.
20. Wang J, Zhang Z, Ying H, Han G, Han WQ. In-situ formation of LiF-rich composite interlayer for dendrite-free all-solid-state lithium batteries. *Chem Eng J*. 2021;411:128534.
21. Zhang S, Liang T, Wang D, et al. A stretchable and safe polymer electrolyte with a protecting-layer strategy for solid-state lithium metal batteries. *Adv Sci*. 2021;8:2003241.
22. Zhang C, Zhang L, Ding Y, et al. Progress and prospects of next-generation redox flow batteries. *Energy Storage Mater*. 2018;15:324-350.
23. Naren T, Kuang GC, Jiang R, et al. Reactive polymer as artificial solid electrolyte interface for stable lithium metal batteries. *Angew Chem Int Ed*. 2023;62:e202305287.
24. Li NW, Shi Y, Yin YX, et al. A flexible solid electrolyte interphase layer for long-life lithium metal anodes. *Angew Chem Int Ed*. 2018;57:1505-1509.
25. Fan X, Chen F, Zhang Y, et al. Constructing a LiPAA interface layer: a new strategy to suppress polysulfide migration and facilitate  $\text{Li}^+$  transport for high-performance flexible Li-S batteries. *Nanotechnology*. 2020;31:095401.
26. Wang Z, Liu J, Wang M, Shen X, Qian T, Yan C. Toward safer solid-state lithium metal batteries: a review. *Nanoscale Adv*. 2020;2:1828-1836.
27. Liu Y, Xu X, Jiao X, et al. LiXGe containing ion-conductive hybrid skin for high rate lithium metal anode. *Chem Eng J*. 2019;371:294-300.
28. Huang S, Long K, Chen Y, et al. In situ formed tribofilms as efficient organic/inorganic hybrid interlayers for stabilizing lithium metal anodes. *Nano Micro Lett*. 2023;15:235.
29. Huang S, Wu Z, Johannessen B, et al. Interfacial friction enabling  $\leq 20 \mu\text{m}$  thin free-standing lithium strips for lithium metal batteries. *Nat Commun*. 2023;14:5678.
30. Zhang H, Liao X, Guan Y, et al. Lithiophilic-lithiophobic gradient interfacial layer for a highly stable lithium metal anode. *Nat Commun*. 2018;9:3729.
31. Liang X, Pang Q, Kochetkov IR, et al. A facile surface chemistry route to a stabilized lithium metal anode. *Nat Energy*. 2017;2:17119.
32. Jiang Z, Jin L, Han Z, et al. Facile generation of polymer-alloy hybrid layers for dendrite-free lithium-metal anodes with improved moisture stability. *Angew Chem Int Ed*. 2019;58:11374-11378.
33. Ward AL, Doris SE, Li L, et al. Materials genomics screens for adaptive ion transport behavior by redox-switchable microporous polymer membranes in lithium-sulfur batteries. *ACS Cent Sci*. 2017;3:399-406.
34. Merna J, Vlček P, Volkis V, Michl J.  $\text{Li}^+$  catalysis and other new methodologies for the radical polymerization of less activated olefins. *Chem Rev*. 2016;116:771-785.
35. Guo R, Gallant BM.  $\text{Li}_2\text{O}$  solid electrolyte interphase: probing transport properties at the chemical potential of lithium. *Chem Mater*. 2020;32:5525-5533.
36. Li S, Wang XS, Li QD, et al. A multifunctional artificial protective layer for producing an ultra-stable lithium metal anode in a commercial carbonate electrolyte. *J Mater Chem A*. 2021;9:7667-7674.
37. Yan K, Lee HW, Gao T, et al. Ultrathin two-dimensional atomic crystals as stable interfacial layer for improvement of lithium metal anode. *Nano Lett*. 2014;14:6016-6022.

## SUPPORTING INFORMATION

Additional supporting information can be found online in the Supporting Information section at the end of this article.

**How to cite this article:** Lai J, Tan R, Jiang H, et al. Development of an in situ polymerized artificial layer for dendrite-free and stable lithium metal batteries. *Battery Energy*. 2024;3:20230070. doi:10.1002/bte2.20230070